# Hybrid cold and hot-wall reaction chamber for the rapid synthesis of uniform graphene

Arjmandi-Tash, H.; Lebedev, N.; Deursen, P.M.G. van; Aarts, J.; Schneider, G.F.

# Hybrid cold and hot-wall reaction chamber for the rapid synthesis of uniform graphene

Hadi Arjmandi-Tash [a], Nikita Lebedev [b], Pauline M.G. van Deursen [a], Jan Aarts [b], Grégory F. Schneider [a, *]

[a] Leiden University, Faculty of Science, Leiden Institute of Chemistry, Einsteinweg 55, 2333 Leiden, The Netherlands
[b] Leiden University, Faculty of Science, Leiden Institute of Physics, Niels Bohrweg 2, 2333 Leiden, The Netherlands

## A R T I C L E   I N F O

## A B S T R A C T

We introduce a novel modality in the CVD growth of graphene which combines cold-wall and hot-wall reaction chambers. This hybrid mode preserves the advantages of a cold-wall chamber such as fast growth and low power consumption, while boosting the quality of growth, similar now to conventional CVD with in hot-wall chambers. The synthesized graphene forms a uniform monolayer. Electronic transport measurements indicate significant improvement in charge carrier mobility compared to graphene synthesized in a cold-wall reaction chamber. Our results promise the development of a fast and cost-efficient growth of high quality graphene, suitable for scalable industrial applications.

© 2017 The Authors. Published by Elsevier Ltd. This is an open access article under the CC BY-NC-ND license (http://creativecommons.org/licenses/by-nc-nd/4.0/).

## 1. Introduction

Cold-wall chambers (CWC) are advantageous for the growth of graphene as they are fast and cost-efficient. The set-up is constructed in a compact manner and the small size of the reaction chamber allows lower gas consumption. In such chambers, the heating energy selectively heats up the specimen, i.e. a copper foil in contact with the hot stage, optimizing energy efficiency and thus reducing growth costs [1]. On the other hand, knowledge of and experience with the chemical vapor deposition (CVD) of graphene in CWC is relatively sparse. Successful reports on the growth of graphene in CWC are rare in comparison with tube oven systems, i.e. hot-wall chambers (HWCs) [1–4]. The sparsity of reports accounts for a general sense of distrust in the community regarding the utilization of CWCs. This manuscript studies the CVD growth of graphene in a CWC; we identify the origin of imperfections and offer solutions to improve the quality of the synthesized graphene, including improved growth parameters and adoption of the growth principle of the HWC, in other words hybridizing CWC and HWC. The modifications are successful in boosting the uniformity and electronic transport properties of the synthesized graphene, which are now comparable with graphene grown in conventional HWCs.

## 2. Comparison of the CWC and HWC

Fig. 1 compares typical CWC and HWC setups. In the HWC, the heating elements are placed outside the chamber tube; heat radiation entering the transparent quartz tube heats up the specimen (copper foil) placed inside the tube (inset in Fig. 1-b). Typically, the heating element is embedded in a large block of an insulating material to minimize energy dissipation to the environment. This block, however, acts as a thermal mass which delays both the heating (to start the growth) and the cooling (at the end of the process) of the chamber. In a CWC, on the other hand, the specimen is placed directly on a resistively heated stage inside the chamber (inset in Fig. 1-a). In typical designs, the size of the heating stage can be as small as the size of the specimen with no insulating materials required, which makes fast processing possible. The two chamber designs find their main difference in their heating regime: uniform radiation in a HWC provides a heating zone larger than the specimen with a uniform temperature whereas the CWC provides heating selectively to the specimen, giving rise to a considerable thermal gradient between the hot stage (T > 1000 °C) and the cold walls (T ~ few tens of °C) during the operation of the CWC (inset Fig. 1-a and b). Fig. 2-a and b characterize graphene grown in a CWC. For this growth, we adopted a recipe similar to what has been developed earlier [1,2,5]; we shall refer to this recipe as "conventional recipe", detailed in Methods. In short, the recipe includes: i) heating the copper foil to 1035 °C, ii) annealing for 10 min and iii)

* Corresponding author.
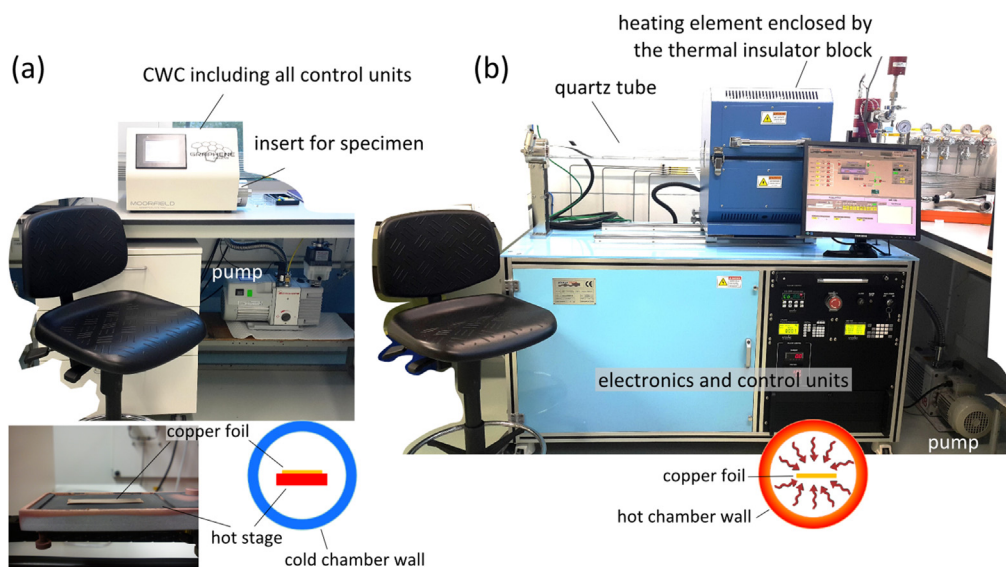  E-mail address: g.f.schneider@chem.leidenuniv.nl (G.F. Schneider).

**Fig. 1.** Cold- versus hot-wall reaction chambers for the growth of graphene. a) Photograph of a commercially available cold-wall chamber (nanoCVD-8G, Moorfield Nanotechnology): The main unit has the dimensions of 40.5 cm × 41.5 cm × 28 cm and weighs 27 kg. The bottom-left inset shows the hot-stage (4.0 cm × 2.5 cm) hosting a copper foil. b) Photograph of a commercially available hot-wall chamber (planarGROW-2B, planarTECH): The unit has the dimensions of 1.75 m × 1.60 m × 0.75 m and weighs ~200 kg.

growth by flow of methane/hydrogen gas mixure in 7:2 ratio for 3 min. The synthesized graphene covers the surface of the copper foil completely, yet suffers from several imperfections, summarized in Table 1:

**Table 1**
Imperfections of chemically synthesized graphene in a CWC.

| Imperfection | Possible origin | Possible solution |
|---|---|---|
| multilayer areas | presence of the defect sites on Cu | increasing the annealing duration |
| | excessive carbon precursor | lowering $CH_4/H_2$, shortening the growth |
| pronounced Raman D peak | contaminations in the supplies | using higher quality supplies |
| | oxidation during transferring | optimizing the transfer process |
| heterogeneous growth | non-uniform heating | hybridizing the CWC and HWC |

The presence of multilayer areas is the first imperfection, evident as rounded or linear patches of different contrasts in Fig. 2-a. Indeed those multilayer islands are nucleated at the defect sites on the copper foil and grow in the presence of excess carbon precursors [6]. Prolonging the annealing step up to 1 h lowers the defect site density by improving the surface quality of the copper. Lowering the $CH_4/H_2$ ratio diminishes the excess of carbon precursors. We note that a much lower $CH_4/H_2$ ratio of 2 sccm/1000 sccm achieved a uniform monolayer coverage in a HWC process [6].

Local crystalline defects, revealed by the prominent D peak in the Raman spectrum form the second type of imperfection (Fig. 2b). Impurities in the utilized gases and/or the oxidation during transfer to the wafer are among potential sources of the D peak in CVD graphene. Solutions can be found by improving the purity of gases and optimizing the transfer process.

Heterogeneous growth and crystalline quality is the last imperfection, evident from dissimilar Raman spectra recorded at different spots on the sample. The heterogeneity persisted even after prolonged annealing to improve the uniformity of the copper

foil. The long quartz tube used in the HWC ensures steady, laminar flow of gases where they reach the copper foil [7]; the absence of such a "guide" in the short reaction chamber may cause local eddies and non-uniform stream. The huge thermal gradient between the hot stage and the walls of the chamber and non-uniform heating due to the small heating zone are additional potential sources of the inhomogeneity. Indeed this imperfection can be viewed as an intrinsic side effects of the compact and energy-efficient design of the CWCs.

## 3. Hybridizing the cold and hot wall growth principles

A way to overcome the side effects of the compact design is to cover the stage with a quartz plate, leaving a gap of about 2 mm for the flow of gases over the copper foil (Fig. 2-c). The benefit is twofold: the flow of the gases through the gap is inside the laminar boundary layer associated with the quartz cap; hence is uniform [7,8]. Secondly, in this design, the heat radiating from the hot stage during the growth is reflected back to the copper foil by the reflective surface of the quartz plate; hence, effectively, a small reaction chamber forms that takes the best features from the CWC and HWC designs. Fig. 2-d and e present optical microscopy, SEM and Raman characterization of graphene synthesized with the improved recipe in the hybrid C/HWC. It is clear that the modifications in the growth recipe and the growth mode (detailed in the Supplementary Materials, section 1) improve the uniformity of growth and prevent onset of multilayer formation. Although there is still a D peak in the Raman spectra, the lower $I_D/I_G$ ratio indicates an improved crystalline structure. The inset in Fig. 2-e focuses on a selected spectrum between 1200 cm$^{-1}$ and 1700 cm$^{-1}$. D, G and D′ peaks are de-convoluted by means of Gaussian fits. We estimated $I_D/I_{D'} = 2.75$, close to the value reported for the grain boundary defects [9] indicating that the synthesized graphene suffers from a high population of grain boundaries, i.e. small grains. The complementary electron diffraction pattern of a suspended graphene sample (Fig. 2-f) shows the presence of regions without any preferred lattice orientation, i.e polycrystalline graphene (visible as the extra diffraction points next to the characteristic diffraction pattern of monolayer graphene). Note that Raman spectra with
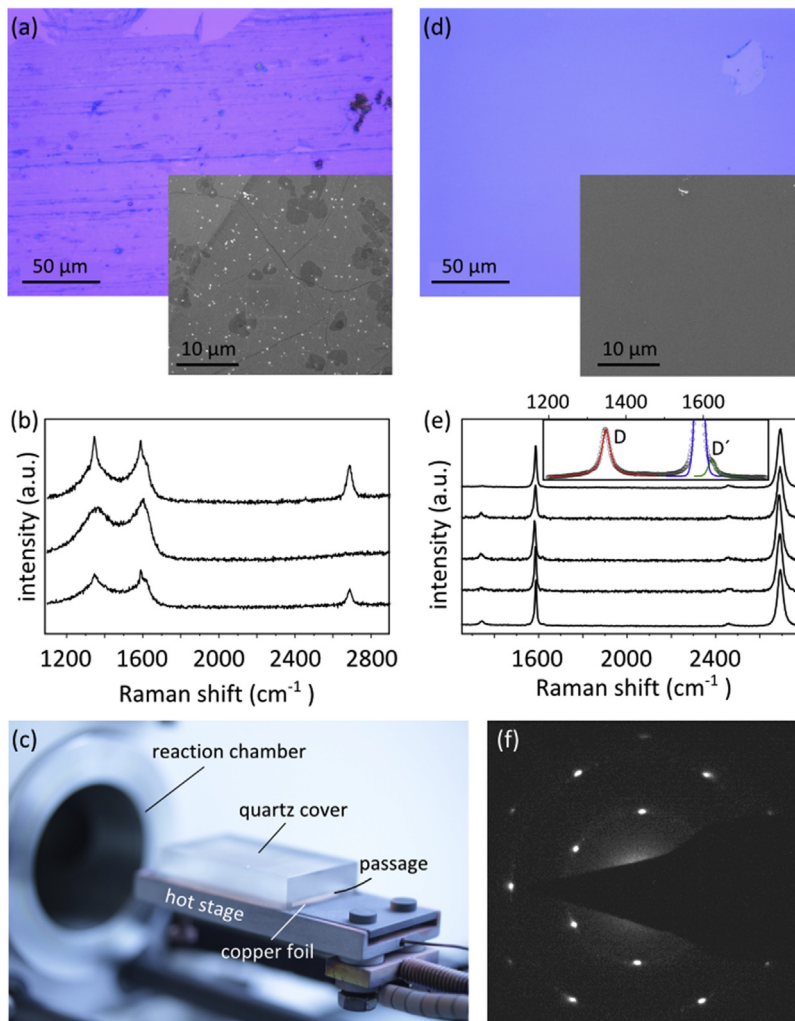
**Fig. 2.** Characterization of graphene samples synthesized via CWC and hybrid C/HWC. a) Typical optical micrograph and scanning electron microscopy images of a graphene sheet synthesized via a conventional recipe for the growth in a CWC (detailed in the text), and transferred onto a $SiO_x$/Si wafer. b) Typical Raman spectra corresponding to arbitrary spots on graphene in (a). c) Photograph illustrating the technique to turn a CWC into hybrid C/HWC. d) Typical optical micrograph and scanning electron microscopy images of a graphene sheet synthesized via an improved recipe (detailed in the text), in a hybrid C/HWC, transferred onto a $SiO_x$/Si wafer. e) Typical Raman spectra corresponding to arbitrary spots on graphene in (d). The inset details a frequency window close to the D, G and D′ peaks. f) Typical diffraction pattern corresponding to a free standing graphene grown in the hybrid C/HWC, recorded by the diffraction mode transmission electron microscopy.

similar $I_D/I_{D'}$ were already reported with CWC [1] indicating that small grains are characteristic to graphene grown in the CWC and hybrid C/HWC.

## 4. Electrical characterization

We characterized the electrical performance of graphene grown using our hybrid C/HWC. Black data points in Fig. 3-a illustrate the gate-dependent resistivity of a graphene sample measured at room temperature. The solid line shows the best fit of the well-established model for graphene conductivity ($\sigma$) [10]: $\sigma^{-1} = (ne\mu_c + \sigma_0)^{-1} + \rho_s$. Here $\mu_c$ is the density-independent charge carrier mobility, $e$ is the elementary charge, $\sigma_0$ is the residual conductivity at the Dirac point and $\rho_s$ is the contribution of short-range crystalline defects on the total resistivity. Additionally, $n$ is the charge carrier density estimated considering the parallel-plate capacitance model across the oxidized silicon layer ( $\varepsilon_r =$ 3.9, t = 300 $nm$). Fig. 3-b compares the extracted room temperature values for $\mu_c$ of several graphene samples grown via hybrid C/HWC and conventional CWC with this fit. The samples grown using our

hybrid C/HWC exhibit an average mobility of $1.5 \times 10^3$ cm$^2$/V.s, showing 27% improvement over the samples grown via the conventional recipe ($1.2 \times 10^3$ cm$^2$/V.s). The improvement is attributed to the uniform crystalline structure and suppression of multilayer patches achieved via hybrid C/HWC CVD. Indeed the detrimental effect of multilayer patches on the electronic properties of graphene has been demonstrated before [6]. Cooling down the sample suppresses phonon scattering; improving to $\mu_c$ 2700 cm$^2$/V.s at 2 K (inset Fig. 3-c). This value for the mobility lies below the best record of chemical growth of graphene in HWC [11] which may be attributed to the relatively large presence of grain boundaries (discussed in the previous section). A comprehensive comparison of the mobility of our devices with state of the art reports is presented in the Supplementary Information (section 3).

Analysis of the gate dependent conductivity of the sample at low temperatures reveals the characteristics of defects in the graphene lattice in terms of defect size $R_0$ and defect density $n_d$ via the "Midgap states" model [12]: $\sigma = \frac{2e^2}{h} \frac{k_F^2}{\pi n_d}[\ln (k_F R_0)]^2$. Here, $k_F = \sqrt{\pi n}$ is the Fermi wave vector of graphene. The solid line in Fig. 3-c
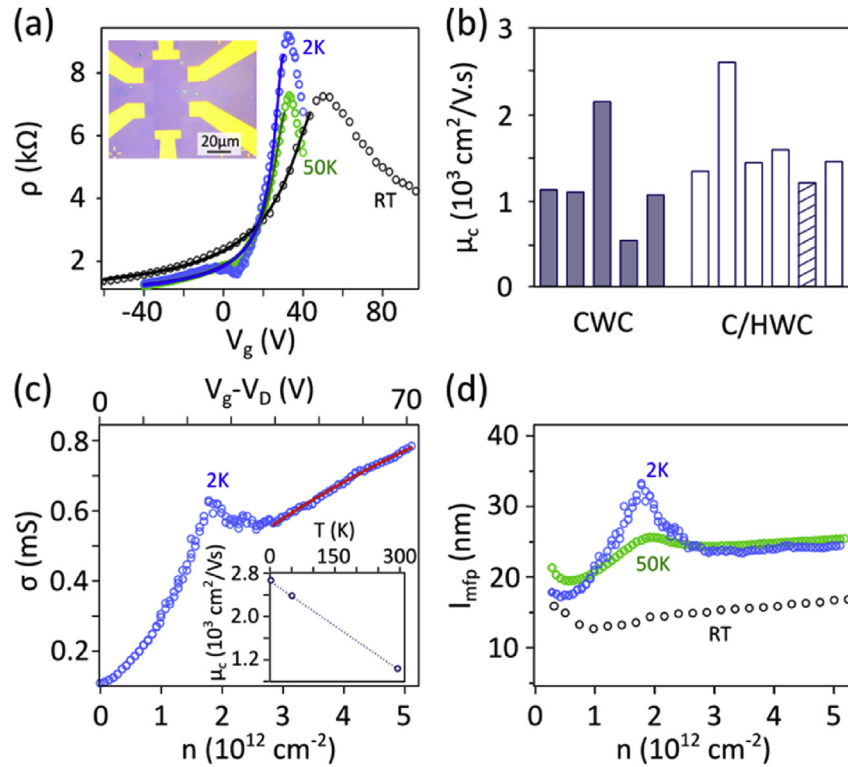
**Fig. 3.** Electric transport properties of graphene grown via hybrid C/HWC. a) Gate dependent electrical resistivity of a sample measured at different temperatures: The solid lines are the best fittings with the model of the conductivity of graphene, discussed in the text. An optical micrograph of the sample is presented in the inset. b) Mobility of different graphene samples synthesized via conventional CWC and hybrid C/HWC; the hatched data point corresponds to the black curve presented in (a). c) Conductivity of the same sample as in (a), measured at 2 K: the solid line is the best fitting with the mid-gap states model. $V_D$ refers to the gate voltage at the Dirac point. The inset plots the mobility of the sample at different temperatures. The dotted line is a guide to the eye. d) Density dependent mean free path of the charge carriers of the sample in (a), at different temperatures.

**Table 2**
Characterization of the crystalline defects in graphene samples.

| Sample | $n_d$ [cm$^{-2}$] | $R_0$ [Å] |
|---|---|---|
| hybrid C/HWC-CVD | $2.1 \times 10^{12}$ | 3.0 |
| HWC-CVD [14,15] | $2.7 \times 10^{12}$ | 1.3 |
| exfoliated graphene [16] | $\leq 1 \times 10^{11}$ | 1.4 |

shows the best fit of this model to the measured conductivity. Due to the short effective range of crystalline defects, their scattering is significant only at a high population of the charge carriers (i.e. far from the Dirac point) [10,13]. Close to the Dirac point the model no longer performs well. Table 2 summarizes the characteristics of the defects revealed by this fit. For the sake of comparison, we included the results reported earlier for CVD graphene grown in a conventional HWC [14,15] and an estimation for exfoliated graphene [16].

Crystalline defect of different types including vacancies, cracks, or grain boundaries contribute to the estimated $R_0$ and $n_d$. Particularly the high population of grain boundaries (with typical sizes larger than single vacancies) in hybrid C/HWC graphene raise the average size of the defects beyond HWC-CVD graphene. The density

of the defects of both hybrid C/HWC and conventional HWC is approximately one order of magnitude higher than that for exfoliated graphene, explaining the poorer transport properties of CVD graphene. The mean free path of charge carriers is estimated as $l_{mfp} = \left( h/2e \right) \mu_{FE} \sqrt{n/\pi}$ where $\mu_{FE} = \sigma/en$ is the field effect mobility of the charge carriers. Fig. 3-d plots the carrier density dependent $l_{mfp}$ at different temperatures. By cooling the sample below room temperature (down to 50 K), the reduction of phonon scattering increases the mean free path. Further reduction of the temperature, however, does not affect the $l_{mfp}$. Particularly at higher carrier density, $l_{mfp}$ saturates about 25 nm which can be attributed to the trapping of the carriers inside graphene grains.

## 5. Conclusion

We presented a systematic study of the CVD growth of graphene in a cold wall chamber. We identified the important imperfections of the grown graphene and proposed solutions to eliminate them. Particularly, a simple technique can turn the CWC into a hybrid C/HWC, considerably improving the uniformity of the growth and the charge carrier mobility. Small grain size remains an important characteristic limiting the transport properties of graphene and poses a challenge for the graphene synthesized in a CWC and hybrid C/HWC.

## 6. Methods

We grew graphene on polycrystalline copper foil (Alfa Aesar,

**Table 3**
Important growth parameters utilized in this work.

| | Annealing duration | Growth duration | Growth temperature | CH$_4$/H$_2$ ratio |
|---|---|---|---|---|
| conventional recipe | 10 min | 3 min | 1035 °C | 7/2 |
| optimized recipe | 90 min | 2 min | 1035 °C | 2/20 |

99.999% purity, 25 μm thickness) in a commercially available cold-wall CVD set-up (nanoCVD-8G, Moorfield Nanotechnology). Briefly, the copper foil is rapidly heated up to 1035 °C and annealed under the continuous flow of hydrogen (20 sccm). Growth starts upon the injection of methane. All gases supplied to the reaction chamber were supplied by Linde Gas. By halting the heating power at the end of the growth phase, the chamber assembly cools down rapidly. We used two different growth recipes, listed in Table 3.

The hybrid cold/hot wall chamber (C/HWC) growth differs from the CWC growth in that during the whole process, the surface of the hot stage and the copper foil was covered by a piece of quartz plate leaving a gap of 1 mm to 2 mm for the gas flow. The quartz plate provides a uniform heating zone to improve the uniformity of the growth.

For optical microscopy and electrical characterizations, we transferred the graphene onto a silicon wafer with a thermally oxidized capping layer of approximately 285 nm. We used well-established recipes [1] for transferring graphene using a supportive poly(methyl methacrylate) (PMMA) layer. SEM characterizations were performed with FEI NANOSEM 200 operating at 10 kV. TEM diffraction patterns were recorded in a FEI Titan cryo-electron microscope operating at 300 kV. Micro-Raman spectroscopy was performed with an inVia Raman Microscope from Renishaw, equipped with a dual-axis XY piezo stage for sample positioning. A laser with 532 nm excitation wavelength and a 100× objective were used. We limited the laser power to below 2 mW to prevent laser induced heating of the samples.

## Acknowledgments

## Appendix A. Supplementary data

Supplementary data related to this article can be found at http://dx.doi.org/10.1016/j.carbon.2017.03.014.

## References

[1] T.H. Bointon, M.D. Barnes, S. Russo, M.F. Craciun, High quality monolayer graphene synthesized by resistive heating cold wall chemical vapor deposition, Adv. Mater 27 (2015) 4200–4206, http://dx.doi.org/10.1002/adma.201501600.

[2] A.I.S. Neves, T.H. Bointon, L.V. Melo, S. Russo, I. de Schrijver, M.F. Craciun, H. Alves, Transparent conductive graphene textile fibers, Sci. Rep. 5 (2015) 9866, http://dx.doi.org/10.1038/srep09866.

[3] V. Miseikis, D. Convertino, N. Mishra, M. Gemmi, T. Mashoff, S. Heun, N. Haghighian, F. Bisio, M. Canepa, V. Piazza, C. Coletti, Rapid CVD growth of millimetre-sized single crystal graphene using a cold-wall reactor, 2D Mater 2 (2015) 14006, http://dx.doi.org/10.1088/2053-1583/2/1/014006.

[4] N. Mishra, V. Miseikis, D. Convertino, M. Gemmi, V. Piazza, C. Coletti, Rapid and catalyst-free van der Waals epitaxy of graphene on hexagonal boron nitride, Carbon N. Y. 96 (2016) 497–502, http://dx.doi.org/10.1016/j.carbon.2015.09.100.

[5] G. Zhang, A.G. Güell, P.M. Kirkman, R.A. Lazenby, T.S. Miller, P.R. Unwin, Versatile polymer-free graphene transfer method and applications, ACS Appl. Mater. Interfaces 8 (2016) 8008–8016, http://dx.doi.org/10.1021/acsami.6b00681.

[6] Z. Han, A. Kimouche, D. Kalita, A. Allain, H. Arjmandi-Tash, A. Reserbat-Plantey, L.L. Marty, S.S. Pairis, V.V. Reita, N. Bendiab, J. Coraux, V. Bouchiat, Homogeneous optical and electronic properties of graphene due to the suppression of multilayer patches during CVD on copper foils, Adv. Funct. Mater 24 (2014) 964–970, http://dx.doi.org/10.1002/adfm.201301732.

[7] J.M. Kay, R.M. Nedderman, Fluid mechanics and transfer processes, Cambridge University Press, 1985.

[8] Victor Lyle Streeter, Fluid mechanics, McGraw-Hill, 1951.

[9] A. Eckmann, A. Felten, A. Mishchenko, L. Britnell, R. Krupke, K.S. Novoselov, C. Casiraghi, Probing the nature of defects in graphene by Raman spectroscopy, Nano Lett. 12 (2012) 3925–3930, http://dx.doi.org/10.1021/nl300901a.

[10] E. Hwang, S. Adam, S. Sarma, Carrier transport in two-dimensional graphene layers, Phys. Rev. Lett. 98 (2007) 186806, http://dx.doi.org/10.1103/PhysRevLett.98.186806.

[11] A. Venugopal, J. Chan, X. Li, C.W. Magnuson, W.P. Kirk, L. Colombo, R.S. Ruoff, E.M. Vogel, Effective mobility of single-layer graphene transistors as a function of channel dimensions, J. Appl. Phys. 109 (2011) 104511.

[12] T. Stauber, N. Peres, F. Guinea, Electronic transport in graphene: a semi-classical approach including midgap states, Phys. Rev. B 76 (2007) 205423, http://dx.doi.org/10.1103/PhysRevB.76.205423.

[13] E. Hwang, S. Adam, S. Das Sarma, Transport in chemically doped graphene in the presence of adsorbed molecules, Phys. Rev. B 76 (2007) 195421, http://dx.doi.org/10.1103/PhysRevB.76.195421.

[14] H. Arjmandi-Tash, D. Kalita, Z. Han, R. Othmen, C. Berne, J. Landers, K. Watanabe, T. Taniguchi, L. Marty, J. Coraux, N. Bendiab, V. Bouchiat, High-yield proximity-induced chemical vapor deposition of graphene over millimeter-sized hexagonal boron nitride, 2017 arXiv:1701.06057, http://arxiv.org/abs/1701.06057 (Accessed 14 February 2017).

[15] H. Arjmandi-Tash, Graphene based mechanical and electronic devices in optimized environments: from suspended graphene to in-situ grown raphene/boron nitride heterostructures, University of Grenoble, 2014.

[16] X. Du, I. Skachko, A. Barker, E.Y. Andrei, Approaching ballistic transport in suspended graphene, Nat. Nanotechnol. 3 (2008) 491–495, http://dx.doi.org/10.1038/nnano.2008.199.